Applied Catalysis A, General 595 (2020) 117510

Contents lists available at ScienceDirect

Applied Catalysis A, General

journal homepage: www.elsevier.com/locate/apcata

Assessment of coke deposits on lamellar metal-modified MFI zeolites in ethylene transformation to aromatic liquids

Laleh Emdadi[a,*], Luther Mahoney[a], Ivan C. Lee[a], Asher C. Leff[a], Wei Wu[b], Dongxia Liu[b], Chi K. Nguyen[c], Dat T. Tran[a,*]

[a] CCDC Army Research Laboratory, Sensors and Electron Devices Directorate, FCDD-RLS-CC, 2800 Powder Mill Road, Adelphi, MD 20783, USA
[b] Department of Chemical and Biomolecular Engineering, University of Maryland, College Park, MD 20742, USA
[c] Department of Chemistry and Life Science, U.S. Military Academy, 646 Swift Road, West Point, NY 10996-1905, USA

ARTICLE INFO

Keywords:
Lamellar zeolite
Metal-modified zeolite
Coke formation
Ethylene conversion
MFI
zeolite

ABSTRACT

The effects of meso-/microporous structure and metal-additive (Ga or Zn) of lamellar MFI catalysts on the characteristics of coke deposits during ethylene-to-aromatic liquids conversion were investigated. The nature, composition, and location of coke deposits in spent lamellar catalysts were analyzed and compared to those on the microporous MFI counterparts, using FTIR, UV–Vis, GC–MS, and argon adsorption-desorption. The total amount of coke and the changes in coke nature during catalyst regeneration were studied by MS/FTIR combined with temperature programmed oxidation. The lamellar meso-/microporous structure of MFI reduces the coke quantity and the heavy coke fractions. The coke preferentially deposites on external surface of lamellar zeolite due to the lower diffusion limitation for bulky coke precursors. Metal-additive changes the catalyst acidity and decreases the coke formation rate, especially when zinc is used. Therefore, the coke formation on zeolite can be tuned by modulating the textural and acidity properties of the metal-modified catalyst.

1. Introduction

Ethylene, one of the most important chemical intermediates in the chemical and petrochemical industry, is mainly produced by steam cracking of fossil-based feedstocks [1–3]. However, the depletion of the fossil energy resources and their harmful environmental effects have promoted the production of ethylene from renewable energy sources such as biomass [4]. Bio-ethanol obtained from fermentation of biomass can be dehydrated to produce ethylene. The resulting ethylene can be transformed to high energy density hydrocarbons through oligomerization, cyclization, and aromatization to be used in the transportation fuel market as a replacement for petroleum-based fuels [5–8].

MFI-type zeolites modified with different metal precursors such as gallium (Ga) and zinc (Zn) are the most widely used catalysts for highly selective conversion of ethylene to aromatics [9–14]. Shape selectivity of the MFI catalyst due to its crystalline microporous structure with 10-membered ring openings (~ 0.5 nm) together with the bifunctional effect of metallic sites and acidic sites of the zeolite provide a high aromatics production yield. The metal loading increases the Lewis acidity of the zeolite catalyst and promotes the dehydrogenation of the acid-catalyzed oligomerization and cyclization products to facilitate the aromatics formation. The nature of the metal, the metal content, and the metal dispersion in the zeolite structure are important parameters affecting the performance of the catalyst [11–13].

Coke formation in zeolite-catalyzed hydrocarbon conversion reactions is one of the major reasons for catalyst deactivation [15–17]. The carbonaceous coke species block the zeolite pores and prevent the diffusion of reactants and products into and out of the zeolite channels or/and poison the active sites of the catalyst during the deactivation process upon coke deposition [18–20]. Catalyst characteristics, operating conditions, and the chemical reaction itself affect the coke structure significantly [21–24]. The formation of coke species inside the micropores (internal coke) and on external surface of zeolites (external coke) involves different reaction steps such as condensation, rearrangement, hydrogen transfer, and dehydrogenation [19,25]. There are many techniques available for characterization of the coke deposits on zeolites [15,23,26–29]. For example, thermogravimetric analysis (TGA) is used to determine the total amount of coke [30,31], while spectroscopic analysis methods such as Fourier transform infrared (FTIR) [21,24,32–34], ultraviolet-visible (UV–Vis) [21,35–37], UV-Raman [38,39], electron spin resonance (ESR) [40], and nuclear magnetic resonance (NMR) [24,29,32,33,41,42], are used to study the nature of the coke. Coke location (internal versus external) can be identified by combination of TGA and gas adsorption-desorption

* Corresponding authors.
E-mail addresses: laleh.emdadi@gmail.com (L. Emdadi), dat.t.tran4.civ@mail.mil (D.T. Tran).

https://doi.org/10.1016/j.apcata.2020.117510
Received 31 August 2019; Received in revised form 8 December 2019; Accepted 3 March 2020
Available online 05 March 2020
0926-860X/

measurements [43–45], while the combination of coke extraction, gas chromatography-mass spectrometry (GC–MS), and transmission electron microscopy (TEM) techniques provides better understanding of the coke composition [42,46–50].

The spent catalyst after formation and deposition of coke species on it can be regenerated by oxidative coke combustion and reused for the catalytic reaction, but such regeneration cycles lead to a gradual loss of crystallinity of the zeolite due to steam treatment at high temperatures and reduce the lifetime of the catalyst for industrial applications [51–53]. Therefore, in addition to the optimization of the reaction conditions, it is necessary to tune the catalyst design parameters for having a better control on coke formation and catalyst regeneration.

The morphology and pore size of the microporous zeolite can affect both the coke amount and coke composition [54]. Zeolites with larger pores usually produce a higher amount of coke that mainly consists of aromatic species [21]. The metal-modification has also been reported to decrease the formation and deposition of carbonaceous coke species responsible for microporous zeolite catalyst deactivation [11,55–57]. More recently, the number of studies showing that zeolite or metal-modified zeolites containing mesoporosity or macropososity in their structure have higher coke resistance and a longer lifetime has been increased [44,48,58–60]. The slower deactivation rate for these hierarchical catalysts is usually correlated to the fast diffusion of coke precursors out of the zeolite structure and an increase of external coke fraction in these catalysts compared to their solely microporous zeolite counterparts. The agglomeration of microporous zeolite crystals with a meso- and macroporous matrix has also been shown to be effective in attenuating the deactivation of the catalyst by coke species [61,62].

The meso- or macro-porosity is usually introduced to the structure of hierarchical zeolites by post-modification methods such as desilication, but controlling the synthesis process for production of uniform meso- or macro-pores is very difficult [63–65]. Another efficient method for production of hierarchical meso-/microporous zeolites with uniform mesopore sizes is synthesis of two-dimensional (2D) lamellar zeolites such as MFI by using organic surfactant molecules as templates [44,66–68]. Metal-modification of 2D lamellar MFI might be an effectual strategy to control the amount, nature, composition, and location of the coke that is formed on the catalyst during hydrocarbon conversion reactions.

In our previous work [69], the effect of metal-modification and lamellar zeolite structure on the catalytic conversion reaction of ethylene-to-aromatic liquids (ETA) was studied. The hierarchical meso-/microporous lamellar MFI was synthesized by the dual template synthesis method developed before [70] and then the zeolite was loaded with Ga or Zn (2 wt.%) using the wet impregnation technique. Catalytic performances of the synthesized Lamellar MFI, 2%Ga-Lamellar MFI, and 2%Zn-Lamellar MFI were analyzed and compared to those obtained for their microporous zeolite counterparts. 2%Zn-Lamellar MFI produced the highest amount of aromatic liquids with the higher selectivity toward mono-benzene alkylated aromatics while a lower fraction of coke precursor species (such as naphthalene) was obtained. The lowest amount of total coke was also obtained for this catalyst based on TGA measurements. The improved performance of this bifunctional catalyst was explained by the combined effect of tuning the textural properties of MFI zeolite through introduction of mesoporosity to its structure and modification of its Brønsted/Lewis acidity ratio by metal-modification which facilitates the aromatics production and also controls the coke formation in the catalyst [69]. The aim of the present work is to analyze the coke deposits and determine the amount, nature, composition, and location of the coke in the above mentioned lamellar zeolite catalysts after ethylene conversion reaction to aromatic liquids over them in comparison to their microporous zeolite analogues. Different techniques, including temperature programmed oxidation (TPO), FTIR, MS, UV–Vis, coke extraction followed by GC–MS, and Ar adsorption-desorption, have been used to better understand the effect of lamellar meso-/microporous zeolite structure and its metal-modification on characteristics of the coke deposits.

2. Experimental

2.1. Catalyst synthesis

Lamellar MFI zeolite was synthesized using the following recipe as reported in our previous publication [70]: $30Na_2O/1Al_2O_3/100SiO_2/10C_{22\text{-}6\text{-}6}/5TPAOH/4000H_2O/18H_2SO_4$. Synthesis steps for $C_{22\text{-}6\text{-}6}$ as structure directing agent, the chemicals that were used, and details of the dual template synthesis technique for lamellar zeolite, template removal by calcination, and ion-exchange of the resulted zeolite have been discussed in the supporting information. Commercial MFI zeolite from Alfa Aesar was used for the purpose of comparison. The commercial MFI in NH_4^+-form and the ion-exchanged lamellar MFI zeolite were activated by heating in air and then impregnated by nitrate solutions of gallium or zinc and calcined to provide metal-modified MFI zeolites with 2 wt.% metal loading as discussed in our previous publication [69]. The details of these synthesis procedures have also been provided in the supporting information. Commercial microporous MFI was designated as Comm MFI for simplicity in nomenclature and six zeolite catalysts including Lamellar MFI, 2%Ga-Lamellar MFI, 2%Zn-Lamellar MFI, Comm MFI, 2%Ga-Comm MFI, and 2%Zn-Comm MFI were used for catalytic conversion reaction of ethylene to aromatic liquids.

2.2. Catalytic conversion of ethylene into aromatic liquids

The ETA reaction was carried out in a packed bed quartz reactor over 1 g catalyst including a mixture of MFI zeolite and silicon carbide at 50/50 wt.% ratio. After pre-treatment of the catalyst at 650 °C under oxygen for 4 h, the reaction was started at 400 °C using a mixture of 5 sccm ethylene and 1 sccm nitrogen gases as reported in our previous publication [69]. The condensable gaseous products were collected as liquid at 4 °C and analyzed by GC–MS (Agilent Technologies 5977 A MSD 7890 B), while the remaining gas products were identified by a 4 channel micro-GC (Agilent Technologies 3000) with a thermal conductivity detector (TCD). More information about the reaction set-up and conditions can be found in the supporting information. After 8 h on stream, the spent zeolite catalysts used for ETA reaction were collected and analyzed using multiple techniques as follows.

2.3. Coke characterization

FTIR spectra of the spent catalysts were obtained using a Harrick Praying Mantis™ high temperature reaction chamber placed inside a Praying Mantis™ Diffuse Reflectance Accessory (Harick Scientific Products, Inc.) in the sample compartment of a Bruker Vertex 70 FTIR spectrometer equipped with a liquid nitrogen cooled MCT detector. The sample cup of the reaction chamber was filled with approximately 75 mg of the spent zeolite catalyst for each experiment and the FTIR spectrum was collected with a spectral resolution of 2 cm^{-1} and 75 scans per spectrum under 80 mL min^{-1} Ar gas (Ultra Pure Grade, Airgas).

UV-Vis spectra were collected using a Perkin-Elmer Lambda 650 S UV–Vis spectrometer, equipped with 60 mm coated Specta-long integrating sphere from LabSphere, over the 200 − 800 nm wavelength range at a scan rate of 2 degrees per minute. The measurements were performed on 75 mg of each spent zeolite catalyst placed in a quartz sample holder. The resulting absorbance spectrum for this spent catalyst was then converted using the Kubelka-Munk function and by subtracting the spectrum of fresh catalyst from it, the UV–Vis spectrum of the coke was determined.

The same FTIR experimental set-up described before was used to carry out the combined MS/FTIR-TPO analysis for the spent zeolite catalysts. In this case, a Fisher Scientific Isotemp 3016 water chiller and

a mass flow controller (MKS Instruments 1179A Mass-FLO®) were utilized to cool the reaction chamber and to regulate the flow rates of feed gases to the high temperature reaction chamber, respectively. The samples were first pretreated at 100 °C for 1 − 2 h under the flow of 80 mL min^{-1}Ar (Ultra Pure Grade, Airgas) to remove the adsorbed water on zeolite, and then cooled down to 25 °C to collect the background spectrum. After that, the oxygen (Ultra High Purity Grade, Airgas) was introduced to the reactor with a flow rate of 20 mL min^{-1}, following a temperature ramp of 25 °C min^{-1} up to 750 °C. This temperature was maintained for 40 min for complete oxidation-combustion. The spectra were collected with a spectral resolution of 2 cm^{-1} and 75 scans per spectrum, while the carbon dioxide (CO_2) and carbon monoxide (CO) gases exiting the catalyst bed during the TPO process were analyzed by an Agilent Technologies 5973 Mass Selective Detector. The collected FTIR data were analyzed and reported based on the spectrum of the coke-free sample obtained at 650 °C. The details of MS calibration for interpretation of the MS-TPO measurement results have been provided in the supporting information.

Extraction of the soluble coke from the spent zeolite catalysts was conducted by dissolving 200 mg of spent catalyst in 6 mL of hydrofluoric acid (HF, 40%) and shaking the mixture for 24 h. When the zeolite was completely dissolved, 4 mL of dichloromethane (CH_2Cl_2, > 99.9%) was added to the mixture. Then, the organic phase was filtered and washed with DI water to obtain pH = 5 before analyzing the resulting extract using a GC–MS system (5977A MSD 7890B, Agilent Technologies). The detailed sample preparation and calibration techniques using standard organic solutions for GC–MS analysis have been described in our previous publication [69].

Ar adsorption-desorption measurements were carried out at −186 °C on an Autosorb-iQ analyzer (Quantachrome Instruments). Prior to the adsorption-desorption measurements, samples were evacuated overnight at 200 °C and 1 mm Hg.

3. Results and discussion

3.1. Effect of the zeolite structure and its metal-modification on the coke amount

MS-TPO was employed to determine the coke content of the spent MFI zeolite catalysts in the ETA reaction. The change of CO signal intensity recorded by MS during the TPO process was not significant for any of the studied zeolite samples. MS collected data for CO_2 were used to determine the CO_2 production rate as discussed in the supporting information. The MS-TPO profiles corresponding to the combustion of the coke deposited on the MFI zeolite catalysts have been shown in Fig. 1. Two types of coke were identified for all examined samples: coke I (light coke), which burns at a relatively low temperature range of 300–525 °C (with the maximum combustion peak at ~420 °C), and coke II (heavy coke), in the 525–650 °C temperature range (with the maximum combustion peak at ~590 °C). Coke I is usually assigned to more hydrogenated coke species, while coke II has lower H/C ratio associated with a more developed coke with a graphitic and polycondensed aromatic nature [19,47,71].

The deconvolution of the MS-TPO profiles in Fig. 1 into two Gaussian peaks (as shown with dashed lines), has been used to quantify the total coke content (C_c, weight percent of the coke in the spent catalyst), the fraction of coke I (f_{CI}), and the fraction of coke II (f_{CII}) in different samples. The results have been summarized in Table 1. Total amounts of coke determined from MS-TPO measurements for spent zeolite catalysts are comparable to those obtained from TGA analysis over these samples in our previous publication [69]. Meso-/microporous lamellar MFI zeolites with and without metal-modification produce a lower amount of total coke (3.1–3.7 wt.%) compared to their microporous zeolite counterparts (4.6–5.0 wt.%), while containing higher fractions of coke I. Lamellar zeolites have larger pores (mesopores) due to their unique structures compared to the microporous commercial zeolites, so

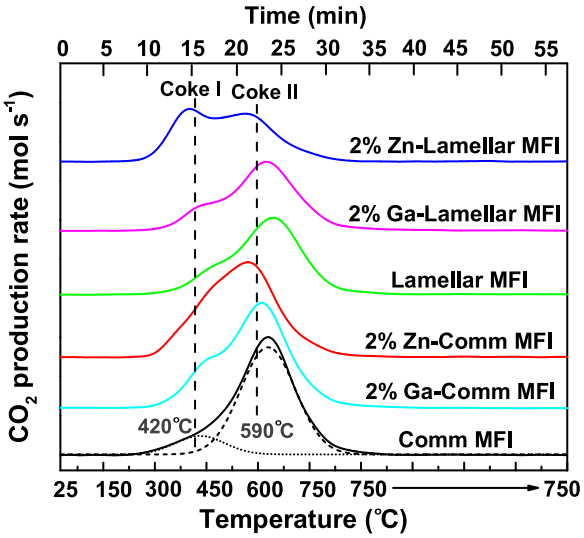

Fig. 1. MS-TPO profiles of the spent MFI zeolite catalysts.

Table 1
Total coke content (C_c), fraction of coke I (f_{CI}), and fraction of coke II (f_{CII}) in spent MFI zeolite catalysts.

Catalyst	C_c (wt.%)[a]	f_{CI} (%)[b]	f_{CII} (%)[b]
Comm MFI	5.0	12.9	87.1
2%Ga-Comm MFI	4.8	16.7	83.3
2%Zn-Comm MFI	4.6	19.1	80.9
Lamellar MFI	3.7	16.0	84.0
2%Ga-Lamellar MFI	3.4	18.5	81.5
2%Zn-Lamellar MFI	3.1	25.8	74.2

[a] Calculated from C_c = ((n_{CO2} x 12)/(weight of spent catalyst)) x 100, n_{CO2} is the total mole of CO_2 evolved from the coke combustion of the spent catalyst during the TPO process, weight of spent catalyst = 0.075 g.

[b] f_{CI} and f_{CII} calculated from deconvolution of the MS-TPO peaks for each catalyst in Fig. 1 assuming that f_{CI} + f_{CII} = 100.

coke precursors formed during ethylene conversion to aromatics have lower diffusion limitations for migration to the external surface of the zeolite that can decrease the formation rate of heavy coke species and make the zeolite catalyst more resistant to deactivation [44,58,60]. Based on the data reported in Table 1, the metal-modification of zeolites also decreases the total amount of coke deposited on them during the ethylene conversion reaction, increases the fraction of coke I, and decreases the maximum combustion temperature for coke I. Zinc has a more pronounced effect compared to gallium. This can be explained by the effect of metal-modification on moderating the acidity (decreasing Brønsted/Lewis acid site ratio) in zeolites and decreasing the formation rate of heavy coke precursors in them [11]. Zinc had a more uniform dispersion in the studied zeolite structures compared to gallium and decreased the total number of Brønsted acid sites, number of external Brønsted acid sites, and the zeolite Brønsted/Lewis acid site ratio, more than gallium, as shown in our previous publication [69], so it was more effective in preserving the zeolite from coke formation during the reaction. The lower maximum combustion temperature of coke I (~350 °C) observed for 2%Zn-Lamellar MFI compared to 2%Zn-Comm MFI might be due to better distribution of the zinc in the former zeolite [69] because of the presence of larger pores (mesopores) in it [72,73]. 2%Zn-Lamellar MFI also had the lowest amount of total coke (3.1 wt.%) and highest fraction of light coke (coke I, 25.8%) compared to all the studied spent zeolite catalysts. Therefore, it can be concluded that not only the morphology of the zeolite structure, but also its acidity change resulting from adding the metal to its structure influence the coke formation rate in zeolite catalyst and determine the total coke content and nature of the coke deposits (coke I and coke II).

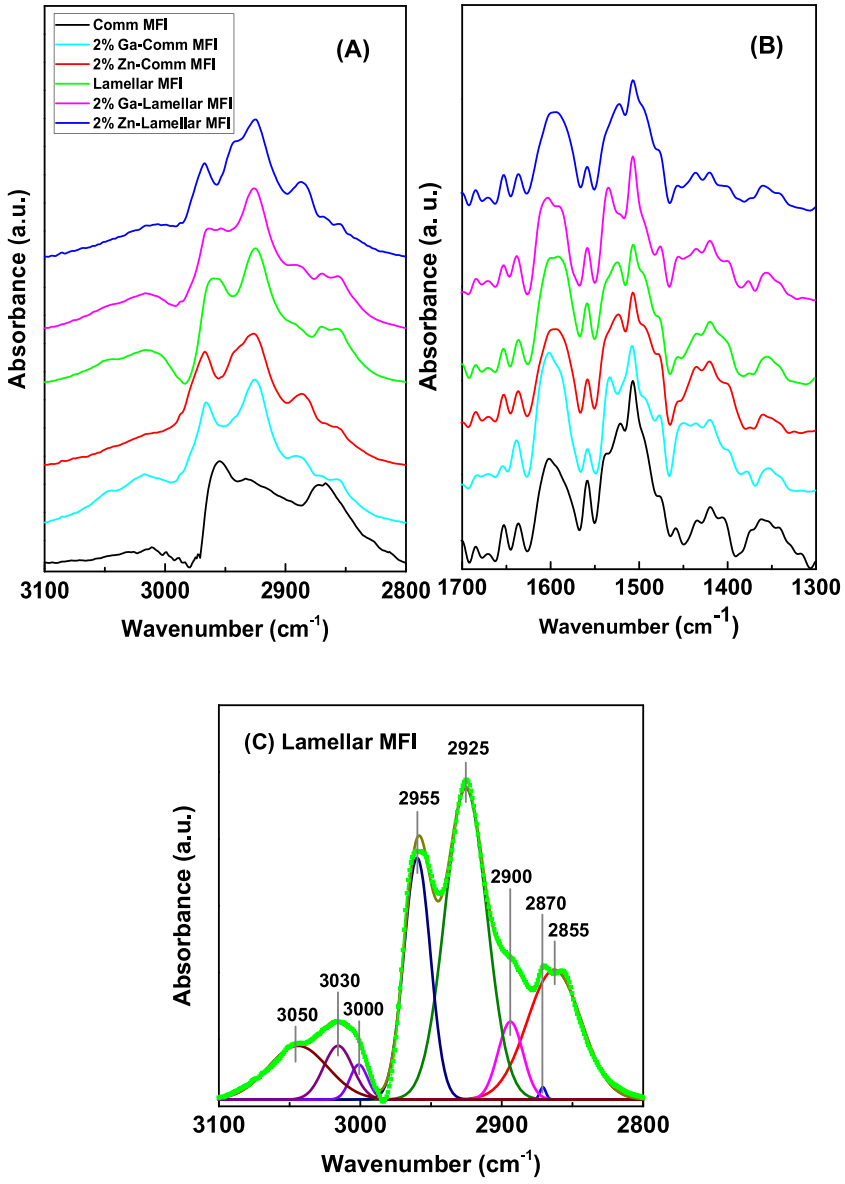

Fig. 2. FTIR spectra of the spent MFI zeolite catalysts in 2800-3100 cm^{-1} region (A) and 1300-1700 cm^{-1} region (B), and deconvolution of the vibrational bands in the 2800-3100 cm^{-1} region for spent lamellar MFI catalyst (C).

3.2. Effect of the zeolite structure and its metal-modification on the coke nature

FTIR spectroscopy was used to study the nature of the coke formed on different zeolite catalysts after 8 h ethylene conversion reaction to aromatic liquids. The presence of coke on zeolites is usually identified by studying the molecular vibrations of hydrocarbon molecules in (i) 2800-3100 cm^{-1} and (ii) 1300 – 1700 cm^{-1} regions of the FTIR spectrum [15,17,74]. The first FTIR region mostly corresponds to the saturated coke species and the second one to the unsaturated coke components. Fig. 2(A) and (B) show the spectra of the spent MFI zeolite catalysts within these two FTIR regions, respectively. In order to quantify the coke vibrations, the spectrum of each spent zeolite catalyst has been deconvoluted into several Gaussian peaks [21] with the following assignments [15,17,75]: 1360 – 1390 cm^{-1}, terminal $-CH_3$ groups related to symmetric aliphatics or branched aliphatics; 1420 – 1490 cm^{-1}, $-CH$, $-CH_2$, and $-CH_3$ groups of asymmetric aliphatics and/or aliphatics linked to aromatics (alkyl aromatics); 1500 – 1540 cm^{-1}, C—C vibrations of alkyl aromatics; 1550 – 1580 cm^{-1}, C—C vibrations of allylic compounds; 1570 – 1590 cm^{-1}, C—C vibrations of polycondensed aromatics; 1600 – 1650 cm^{-1}, C—C vibrations of dienes, olefins, and polyenes; 2855 cm^{-1}, $-CH_2$ groups related to symmetric paraffinic hydrocarbons; 2870 cm^{-1}, $-CH_3$ groups related to symmetric paraffinic hydrocarbons; 2900 – 2920 cm^{-1}, $-CH$ and $-CH_2$ groups of asymmetric paraffinic hydrocarbons; 2955 cm^{-1}, $-CH_3$ groups of asymmetric paraffinic hydrocarbons; 2975 – 3000 cm^{-1}, $-CH$ and $-CH_2$ groups related to symmetric olefinic hydrocarbons; 3030 cm^{-1}, $-CH$ groups of single-ring aromatics or alkyl aromatics; 3050 – 3080 cm^{-1}, $-CH_2$ groups of asymmetric olefinic hydrocarbons.

The total area of the identified coke peaks in 1300 – 1700 cm^{-1} and 2800 – 3100 cm^{-1} FTIR regions for each zeolite catalyst, calculated by integration of the area under these peaks, decreases from 22.4–22.0, 20.9, 20.6, 17.5, and 16.3 for Comm MFI, 2%Ga-Comm MFI, 2%Zn-Comm MFI, Lamellar MFI, 2%Ga-Lamellar MFI, and 2%Zn-Lamellar MFI, respectively. This trend is similar to the one observed for the total coke content measured by MS-TPO method for these zeolites (Table 1), confirming the accuracy of the results obtained from MS-TPO analysis.

Fig. 2(C) demonstrates the deconvolution of the peaks in 2800 – 3100 cm^{-1} region of the FTIR spectrum for the spent Lamellar

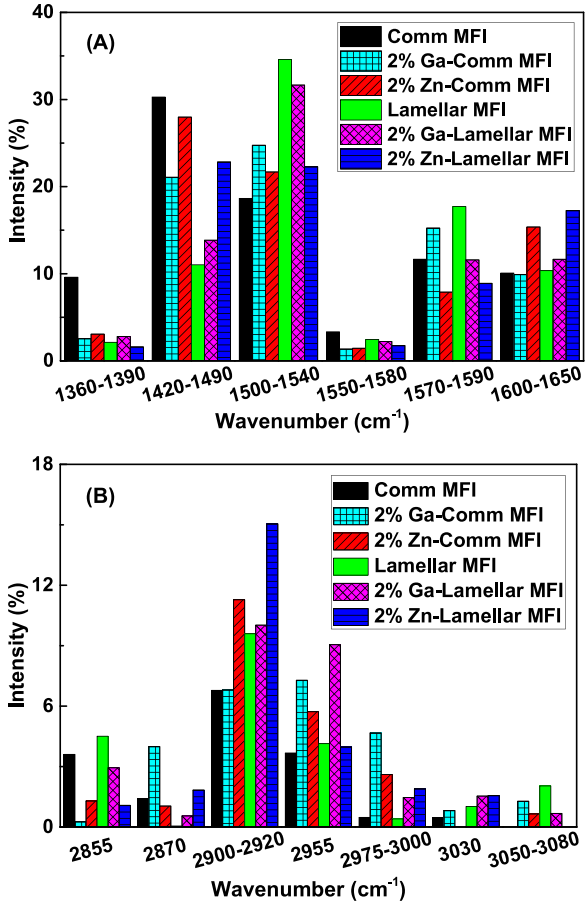

Fig. 3. Fraction of intensities (calculated using the area of the peaks in Fig. 2) of several characteristic vibrational bands corresponding to spent MFI zeolite catalysts in the FTIR region 1300-1700 cm^{-1} (A) and 2800-3100 cm^{-1} (B), respectively.

MFI catalyst as an example. The bands of $-CH$, $-CH_2$, and $-CH_3$ groups (2925 cm^{-1} and 2955 cm^{-1}) have the highest intensity showing the paraffinic nature of the coke formed on Lamellar MFI catalyst. The results of deconvolution of the FTIR peaks, integrating the area of the resulted Gaussian peaks, and normalizing the areas by the total area of the identified vibrations (fraction of intensity) have been shown in Fig. 3(A) and (B) for 1300 – 1700 cm^{-1} and 2800 – 3100 cm^{-1} FTIR regions, respectively.

As it can be seen in Fig. 3(A) and (B), for all the spent zeolite catalysts, the most intense bands are observed in 1420 – 1540 cm^{-1} FTIR region, corresponding to the aliphatics, aliphatics linked to aromatics, and alkyl aromatics. The metal-modified zeolites produced lower fractions of polycondensed aromatics (1570 – 1590 cm^{-1}) and higher fractions of olefins (1600 – 1650 cm^{-1}) compared to their unmodified zeolite counterparts, while the effect of zinc was more significant than that of the gallium [69]. Decreasing the accessibility to Brønsted acid sites (by decreasing the number of total and external Brønsted acid sites) and Brønsted acidity strength of the metal-modified zeolites (by decreasing the Brønsted/Lewis acid sites ratio) [69] that promotes the formation of lighter coke precursors can justify this observed trend [76]. Moreover, it should be noted that, the metal-modification in commercial zeolites increases the fraction of alkyl aromatic coke species, while the opposite trend is observed for lamellar zeolites. This should be due to the structure of lamellar zeolites with larger pores and higher accessibility index for relatively large molecules (determined in our previous publication) [69] that facilitates the diffusion of the aromatic coke precursors out of the zeolite micropores in comparison to the microporous commercial zeolites which can trap these coke precursors for a longer time and convert them to alkylated aromatic coke species.

Fig. 3(B) shows that in 2800 – 3100 cm^{-1} FTIR region, the intensity of the bands assigned to $-CH$, and $-CH_2$ groups of asymmetric paraffinic hydrocarbons (2900 – 2920 cm^{-1}) is the highest for all the studied zeolite catalysts. Metal-modification of the zeolite structures increases the production of these paraffinic coke species especially when zinc is used. At the same time, the intensities of the bands in 2975 – 3000 cm^{-1} and 3030 cm^{-1} FTIR ranges related to the olefinic and single-ring aromatic coke species, respectively, increase by adding the metal to the zeolite structure. Since the intensities of vibrational bands in the 1300 – 1700 cm^{-1} FTIR range (Fig. 3(A)) are significantly higher than those in the 2800 – 3100 cm^{-1} FTIR range (Fig. 3(B)), it can be concluded that a large portion of the coke deposited on the studied MFI zeolite catalysts has an unsaturated nature.

The chemical nature of the coke components deposited on the spent zeolite catalysts used for ethylene conversion reaction to aromatic liquids was further analyzed by UV–Vis spectroscopy. This method uses an electron beam with higher energy compared to FTIR technique enabling the detection of coke species based on the differences in electronic transition of molecular orbitals and providing high sensitivity to coke species with conjugated double bonds and unsaturated carbenium ions [77]. Fig. 4 displays the UV–Vis spectra for the spent MFI zeolite catalysts in the 200 – 800 nm range. The broad coke bands observed for different zeolite catalysts except for 2%Zn-Lamellar MFI show the heterogeneity of the coke molecules formed during the ethylene conversion reaction. The UV–Vis coke bands in the 220 – 265 nm range are usually assigned to dienes, cyclohexadienes, benzenes, and conjugated dienic species as coke precursors while 315 – 375 nm bands are attributed to conjugated double bonds or polycondensed aromatics [15,17]. The bands in the 415 – 695 nm range are ascribed to increasingly condensed polyaromatic structures with more than four aromatic rings by increasing the wavelength [17,78].

The fraction of the UV–Vis coke bands at different wavelengths, calculated by deconvolution of the UV–Vis peaks and integration of the area under the resulted Gaussian peaks, for each zeolite catalyst has been reported in Table 2. The highest fraction of the coke for the Comm MFI and Lamellar MFI zeolite catalysts (0.35 and 0.41, respectively) is observed at 695 nm corresponding to the polycondensed aromatics with long chains and modification of the zeolite structure with gallium does not change these fractions much. On the other hand, adding the zinc to the zeolite structure results in formation of shorter chains of polycondensed aromatics as the main constituents of the coke for 2%Zn-Comm MFI (0.4 at 485 nm) and 2%Zn-Lamellar MFI (0.5 at 315 nm) catalysts. These results are consistent with those observed for FTIR spectroscopy (1570-1590 cm^{-1} and 3030 cm^{-1} regions) in Fig. 3,

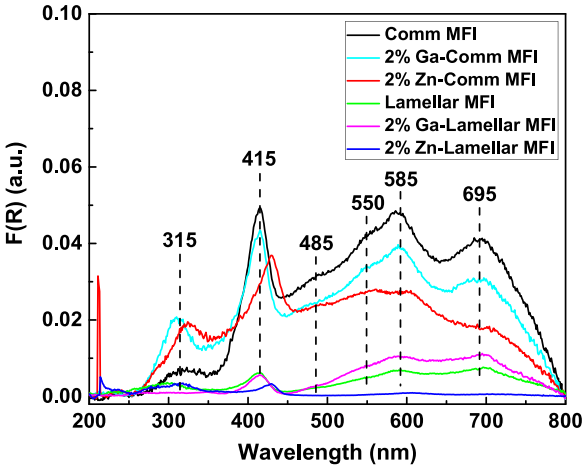

Fig. 4. UV–Vis spectra of the spent MFI zeolite catalysts in 200-800 nm range.

Table 2
Fraction of the coke bands for spent MFI zeolite catalysts in 200-800 nm UV–Vis range.

Catalyst	Fraction of the coke bands at different UV-Vis wavelengths						
	235 nm	315 nm	415 nm	485 nm	550 nm	585 nm	695 nm
Comm MFI	0	0.05	0.17	0.10	0.19	0.14	0.35
2%Ga-Comm MFI	0	0.09	0.22	0.05	0.19	0.16	0.29
2%Zn-Comm MFI	0	0.14	0.06	0.40	0.09	0.11	0.20
Lamellar MFI	0.01	0.15	0.10	0.03	0.11	0.20	0.41
2%Ga-Lamellar MFI	0	0.12	0.05	0	0.11	0.31	0.41
2%Zn-Lamellar MFI	0.05	0.50	0.28	0	0	0.15	0.02

showing that the addition of metal to the zeolite structure decreases the fraction of heavy aromatic coke species and increases the fraction of lighter aromatic compounds by changing the zeolite acid site strength and accessibility [69].

3.3. Effect of the zeolite structure and its metal-modification on evolution of the coke nature during the TPO process

FTIR-TPO was employed to study the evolution of the coke nature during the TPO process by collecting the FTIR spectra at different combustion temperatures [21,79]. Figs. 5 and 6 show the FTIR spectra of the spent MFI zeolite catalysts at different TPO temperatures in $2800-3100\ cm^{-1}$ and $1300-1700\ cm^{-1}$ regions, respectively. The assignment of the coke vibrational bands in these figures is same as that explained in section 3.2. No coke vibrational band was observed at the end of the TPO process in the FTIR spectrum of any of the spent MFI zeolite catalysts, when the temperature was close to the combustion temperature ($600-650\ ^{\circ}C$) of polycondensed aromatics ($1580\ cm^{-1}$), proving that the studied zeolite catalysts were successfully regenerated.

The combination of the FTIR and TPO techniques demonstrates that

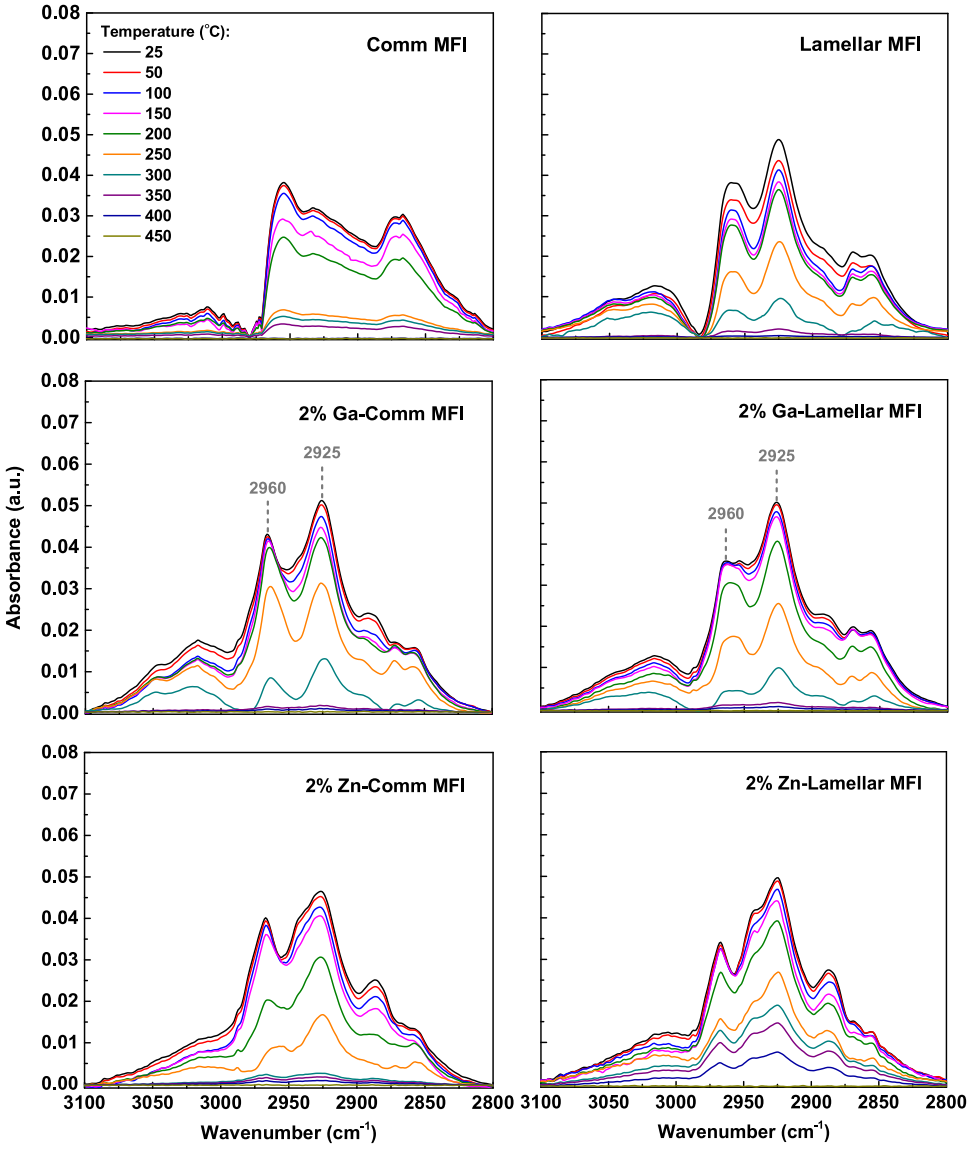

Fig. 5. FTIR-TPO spectra of the spent MFI zeolite catalysts at different combustion temperatures in 2800-3100 cm^{-1} region.

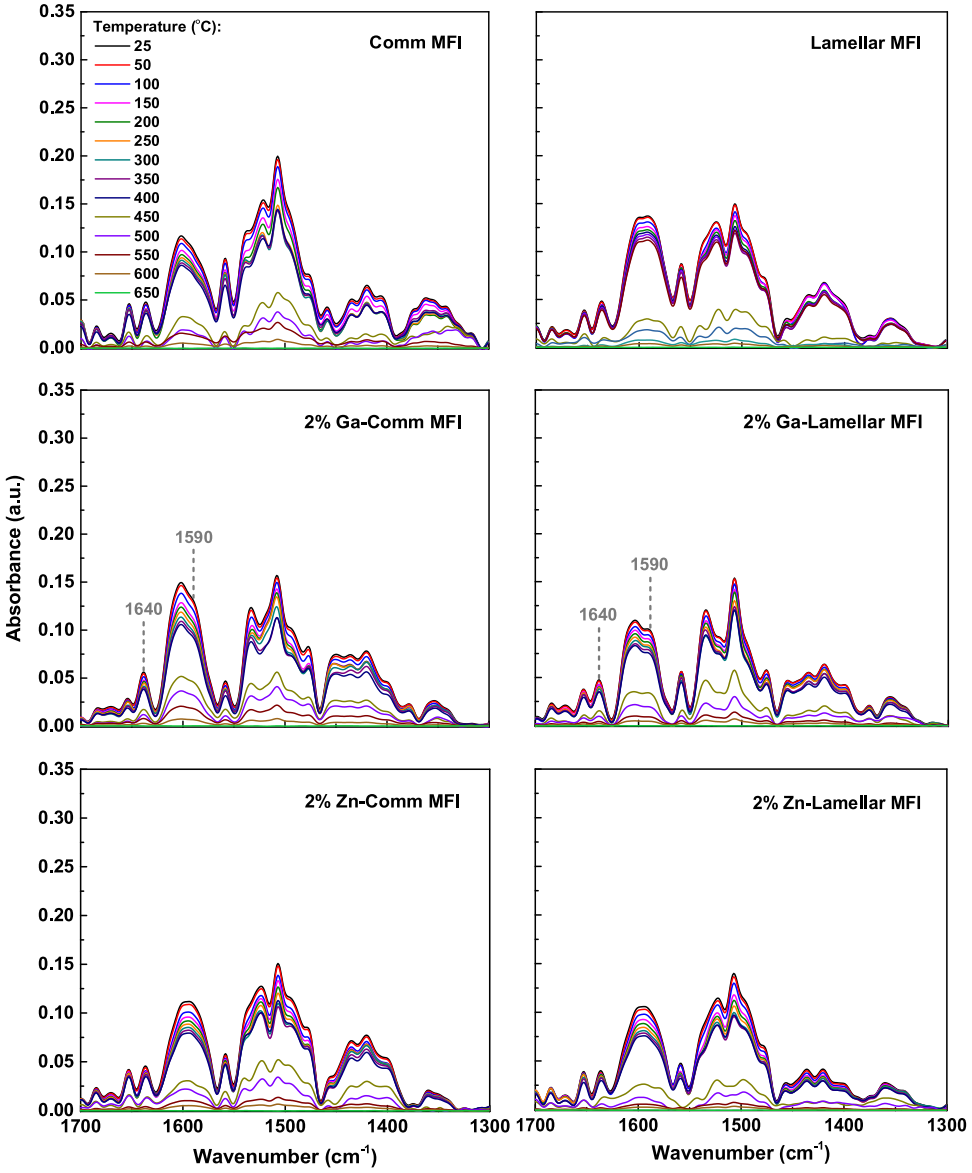

Fig. 6. FTIR-TPO spectra of the spent MFI zeolite catalysts at different combustion temperatures in 1300-1700 cm^{-1} region.

the vibrational bands of paraffinic $-CH$, $-CH_2$, and $-CH_3$ groups in 2855 – 2955 cm^{-1} FTIR region (Fig. 5) disappear at relatively lower temperatures (400 – 450 °C) compared to the bands related to the polycondensed aromatics (1590 cm^{-1}) and unsaturated polyenes (1640 cm^{-1}) in the 1300 – 1700 cm^{-1} FTIR region (Fig. 6) that vanished at 600 – 650 °C. Thus, it can be concluded that the combustion of the coke formed on the spent zeolites during the ethylene conversion reaction to aromatic liquids is selective and depends on the regeneration temperature.

Fig. 7 shows the evolution of the intensities of the selected FTIR vibrational coke bands with time and temperature during the TPO process over the spent MFI zeolite catalysts. The observed trend in this graph confirms the selective combustion of the coke components based on the catalyst regeneration temperature. The paraffinic coke components (2925 cm^{-1} and 2960 cm^{-1}) disappear at lower temperatures compared to polycondensed aromatics (1590 cm^{-1}) or unsaturated polyenes (1640 cm^{-1}). The intensity of the FTIR vibrational band at 1590 cm^{-1} decreases rapidly at temperatures below 200 °C due to the desorption of the ethylene reaction conversion products from the spent catalyst surface which interfere with the FTIR vibrational bands of the coke components. A similar trend observed for all the studied spent zeolite catalysts in Fig. 7 reveals that the structure of the zeolite and its metal-modification does not significantly affect the evolution of the coke nature with temperature during the TPO process.

3.4. Effect of the zeolite structure and its metal-modification on the coke composition

Complete dissolution of the zeolite framework in HF solution followed by coke extraction from spent zeolite catalysts using CH_2Cl_2 and GC–MS analysis of the extracted coke was carried out to gain information about composition of the soluble portion of the coke in CH_2Cl_2 for these catalysts [21,33]. The results are demonstrated in Fig. 8. It can be seen that the highest fraction of soluble coke in all spent catalysts belongs to benzene and naphthalene derivatives and only a small portion of the soluble coke consists of polyaromatics with more than two benzene rings such as anthracenes and phenanthrenes. Traces of other polycyclic aromatics have also been detected. Lamellar zeolites produce higher fractions of single-ring aromatics (benzenes) compared to commercial zeolites and adding metal to the zeolite structure intensifies this effect. The results are in good agreement with the MS results showing the highest fraction of light coke observed for 2%Zn-

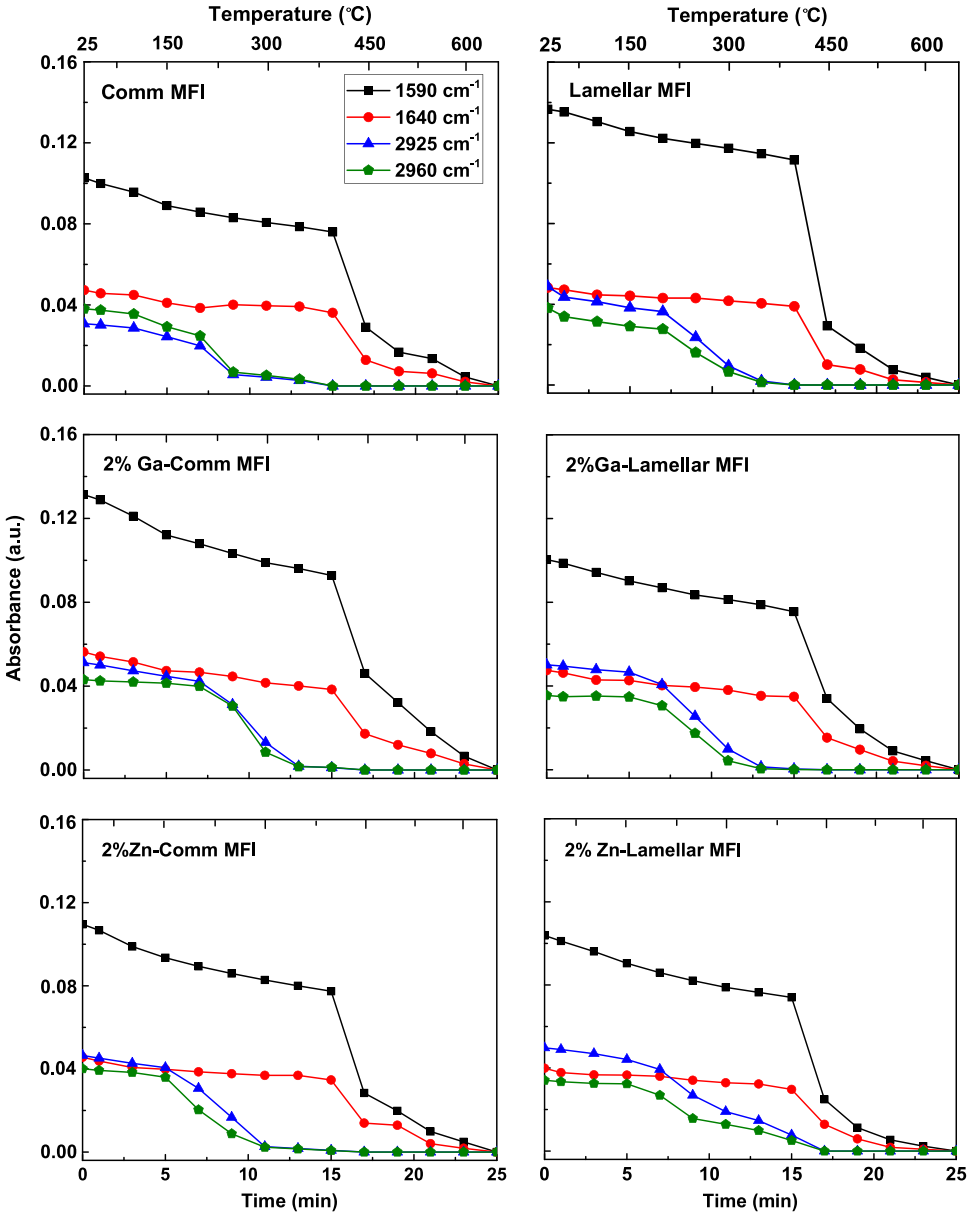

Fig. 7. Combustion profiles of several characteristic vibrational bands (calculated as the maxima of the FTIR peaks) corresponding to the spent MFI zeolite catalysts.

Lamellar MFI catalyst and can be explained based on its meso-/microporous structure with high accessibility to acid sites and low Brønted/Lewis acid ratio (determined in our previous publication [69]) resulting in formation of lighter coke species. Table 3 shows the components representative of each family of the soluble coke extracted from spent zeolite catalysts. The number of carbon atoms attached to the benzene ring are referred as C1 (methyl group) to C6 (six methyl groups or combinations of different carbon groups such as methyl, ethyl, propyl, and butyl that provide six carbon atoms attached to the benzene ring). It can be seen that benzene coke derivatives including one to six carbon atoms attached to the aromatic ring, while naphthalene coke derivatives consist of naphthalene and one to four carbon atoms linked to the aromatic rings. Anthracene and phenanthrene coke derivatives of soluble coke are composed of one and two carbon atoms attached to their aromatic rings, respectively. Other polycyclic aromatics present in soluble coke are made up of tetralin, indan, and indan derivatives with one or two additional carbon atoms. Compositions of the benzenes and naphthalenes groups of the soluble coke are displayed in Fig. 9(A) and (B), respectively. Lamellar MFI zeolites have higher fractions of lighter benzene and naphthalene derivatives with lower number of carbon atoms (C1-C3) attached to their aromatic rings compared to their commercial zeolite counterparts. Adding metal to the zeolite structure, especially zinc (compared to gallium) increases the fraction of these components significantly. These results are in agreement with those obtained by FTIR, UV–Vis, and MS-TPO for spent MFI catalysts. Moreover, it should be noted that the conversion of ethylene to aromatic products over all six studied MFI zeolites was around 99% and did not change over the course of reaction for 8 h [69]. This relatively low deactivation rate observed for these catalysts has been reported before in hydrocarbon cracking reactions of light olefins and correlated to the diffusion of coke precursors towards the external surface of the zeolite crystals due to the unique three-dimensional structure of MFI zeolite [32,47]. The aforementioned differences in coke composition among the studied spent catalysts are also linked to the composition of the ethylene conversion reaction products. Commercial MFI zeolites showed higher selectivity towards polyaromatics as reaction products [69] and the nature of the coke formed over them is mostly heavy benzene alkylated derivatives and polyaromatics. On the other hand,

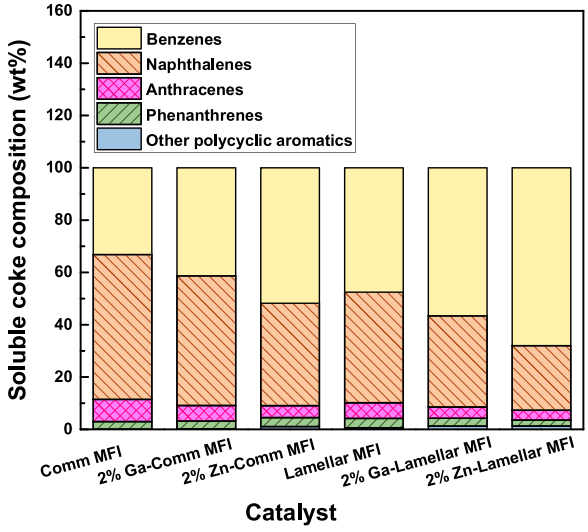

Fig. 8. Composition of the soluble coke extracted from the spent MFI zeolite catalysts.

Table 3
Main components of each family of the soluble coke, extracted from the spent MFI zeolite catalysts.

benzenes	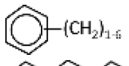
Naphthalenes	
Anthracenes	
Phenanthrenes	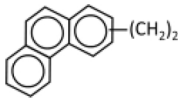
Other polycyclic aromatics	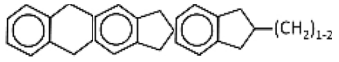

lamellar MFI zeolites had higher selectivity for mono-benzene alkylated aromatics [69] and the main coke components formed over them are light benzene alkylated derivatives, showing the remarkable effect of lamellar meso-/microporous structure to overcome the diffusion limitations for products and coke precursors. Metal-modification intensified this effect by producing more mono-benzene alkylated aromatics [69] and as a results less polyaromatic coke species, emphasizing the effect of metal doping on modification of the acidity of the zeolite which directly affects the formation of products and coke composition on the catalyst.

3.5. Effect of the zeolite structure and its metal-modification on the coke location

Ar adsorption-desorption measurements were carried out to determine the location of the coke formed in the zeolite catalysts used for ethylene conversion reaction to aromatic liquids. Fig. 10(A) and (B) show the Ar isotherms and the nonlocal density functional theory (NLDFT) pore size distributions of the spent MFI zeolite catalysts derived from the adsorption branch of the isotherms, respectively. Ar uptake of each spent zeolite catalyst shown in Fig. 10(A) is much lower and its hysteresis loop is narrower than that measured for the fresh zeolite tested before and reported in our previous publication [69]. The textural properties of the spent MFI zeolite catalysts including their BET surface area (S_{BET}), external surface area (S_{ext}), micropore surface area (S_{micro}), micropore volume (V_{micro}), total pore volume (V_{total}), and

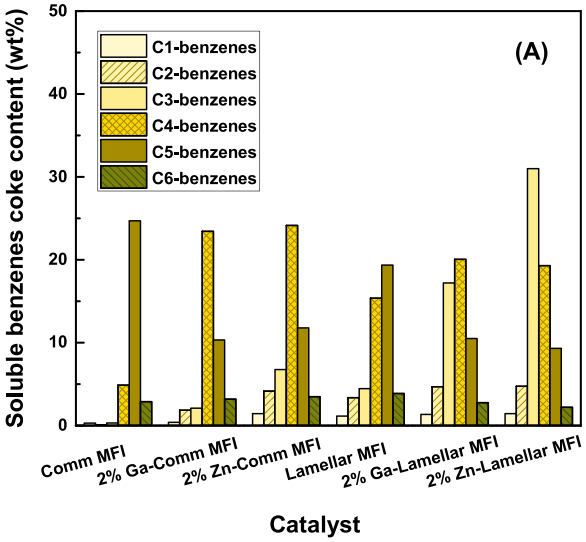

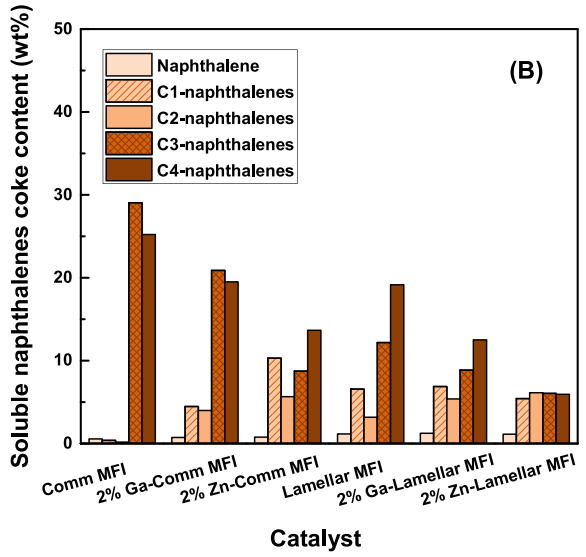

Fig. 9. Compositions of the soluble benzenes coke (A) and naphthalenes coke (B) extracted from the spent MFI zeolite catalysts.

mesopore volume (V_{meso}) have been summarized in Table 4. Fig. 10(B) and Table 4 show that the pore volumes and pore surface areas decrease for spent commercial and lamellar MFI catalysts compared to their fresh zeolite counterparts reported before [69]. The remarkable decrease in Ar uptake and porosity are mainly due to the accumulation of the coke in the zeolite catalysts.

The amount of coke formed in the zeolite micropores (internal coke) was calculated from the decrease in micropore volume of the spent zeolite catalysts as compared to the fresh zeolite samples. The amount of coke formed on the external surface or mesopores of the zeolites (external coke) was calculated by subtracting the internal coke content from the total coke content obtained from MS-TPO measurements. This analysis was based on the assumption that the remaining micropore volume in the spent catalysts was fully accessible to Ar molecules and the coke density was 1.22 g mL^{-1} [44,45,58]. It should be noted that the zeolite samples were diluted with SiC (50/50 wt.%) before running the ethylene conversion reaction over them, so the micropore volume measured for the fresh zeolite ($V_{micro, f}$) should be divided by two in order to represent the microspore volume of each catalyst. The results are shown in Table 5. The fraction of coke in the micropores of the spent catalysts (internal coke) decreases significantly in lamellar MFI

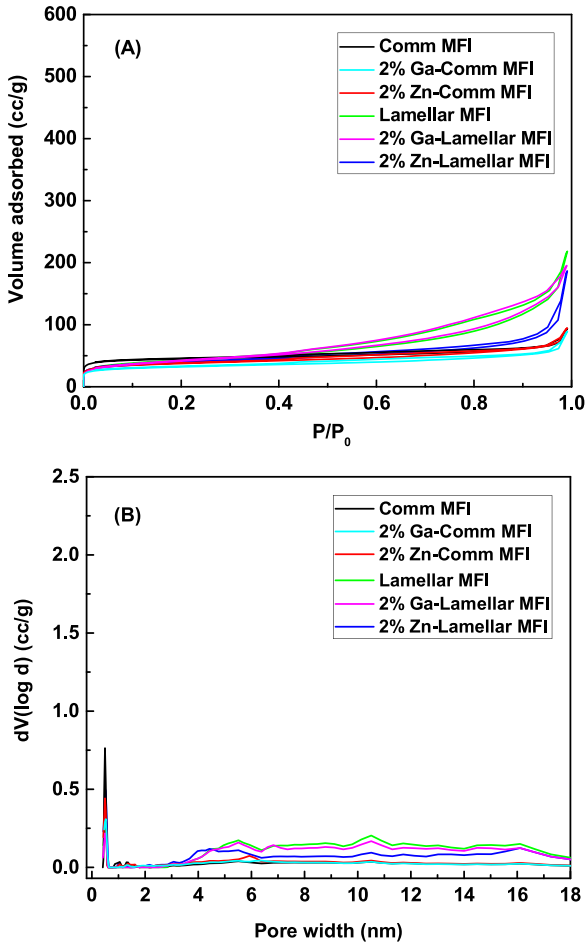

Fig. 10. Ar adsorption-desorption isotherms (A) and the NLDFT pore size distributions (B) of the spent MFI zeolite catalysts.

zeolites (29–53%) compared to their microporous MFI zeolite counterparts (62–77%). This is consistent with the reported data for spent mesoporous zeolites in hydrocarbon conversion reactions and has been correlated to the decrease in the diffusion path lengths and hence facile diffusion of the coke precursors to the external surface of the zeolite by introducing the mesoporosity to its structure [58,59]. 2%Zn-Lamellar MFI has the lowest fraction of internal coke (29%) among all the studied catalysts. This might be due to the combinational effect of the lamellar structure (high mesoporosity and accessibility to Brønsted acid sites) and metal-modification (lower Brønsted/Lewis acid site ratio) of this zeolite [69] on coke formation process in it. Therefore, not only the coke content and its nature, but also coke location in the MFI zeolite catalyst can be controlled by tuning its structure and acidity.

Table 5
Fraction of internal coke and external coke for the spent MFI zeolite catalysts calculated based on Ar adsorption-desorption and MS-TPO measurements.

Catalyst	$V_{micro,\ f}$ [a] ($cm^3\ g^{-1}$)	$V_{int\ coke}$ [b] ($cm^3\ g^{-1}$)	$m_{int\ coke}$ [c] ($g_{int\ coke}\ g^{-1}$)	f_{int} [d] (%)	f_{ext} [e] (%)
Comm MFI	0.115	0.025	0.031	62	38
2%Ga-Comm MFI	0.112	0.030	0.037	77	23
2%Zn-Comm MFI	0.106	0.025	0.031	67	33
Lamellar MFI	0.050	0.012	0.015	41	59
2%Ga-Lamellar MFI	0.049	0.015	0.018	53	47
2%Zn-Lamellar MFI	0.047	0.007	0.009	29	71

[a] Micropore volume of fresh zeolite (without SiC) calculated from *t*-plot method and reported in our previous publication [69].
[b] Volume of the internal coke in spent catalyst $= (V_{micro,f} - (V_{micro} \times 2))/2$, V_{micro} has been reported in Table 3.
[c] Mass of the internal coke in spent catalyst calculated using $m = \rho \times V_{int\ coke}$, ρ (density of the coke) $= 1.22\ g\ mL^{-1}$.
[d] Fraction of the internal coke in spent catalyst calculated from $f_{int} = (m_{int\ coke}/Cc) \times 100$, Cc has been reported in Table 1.
[e] Fraction of the external coke in spent catalyst calculated from $f_{ext} = 100 - f_{int}$.

4. Conclusions

In summary, the effects of meso-/microporous structure and metal addition (Zn or Ga) in lamellar MFI zeolite catalysts on properties of the coke formed in ethylene conversion to aromatic liquids were systematically studied. Meso-/microporous lamellar MFI zeolite was synthesized using the dual template method and then impregnated with gallium or zinc (2 wt.%). Commercial MFI zeolite was also modified by gallium or zinc (2 wt.%) using the same impregnation method for comparison purpose. The spent meso-/microporous Lamellar MFI, 2%Ga-Lamellar MFI, and 2%Zn-Lamellar MFI zeolite catalysts, were examined after 8 h time on stream using a combination of different coke characterization techniques. The results show that metal-modified meso/-microporous lamellar MFI produces the lowest amount of coke and the highest fraction of light coke species compared to all the other spent catalysts. The effect of zinc is much more pronounced than gallium that can be attributed to its more significant effect in decreasing the Brønsted/Lewis acidity of the zeolite and its uniform distribution in the zeolite structure. The coke formed on all spent catalysts has a relatively unsaturated nature mostly consisting of aliphatic, aliphatic linked to aromatics or alkyl compounds. Metal-modification decreases the fraction of polycondensed aromatic coke and increases the fraction of benzene derivatives. The coke combustion in these zeolite catalysts is a selective process and the paraffinic coke species which are relatively lighter than olefinic and polycondensed aromatic coke species burn at lower temperatures. The lamellar zeolites produce a higher fraction of external coke compared to their microporous zeolite counterparts which make them more resistant to deactivation. Thus, by tuning the textural properties of the zeolite catalysts through synthesis of lamellar structures and modulating the acidity properties of them by metal-

Table 4
Textural properties of the spent MFI zeolite catalysts derived from Ar adsorption-desorption isotherms.

Catalyst	S_{BET} [a] ($m^2\ g^{-1}$)	S_{ext} [b] ($m^2\ g^{-1}$)	S_{micro} [b] ($m^2\ g^{-1}$)	V_{micro} [b] ($cm^3\ g^{-1}$)	V_{total} [c] ($cm^3\ g^{-1}$)	V_{meso} [d] ($cm^3\ g^{-1}$)
Comm MFI	114	32	82	0.033	0.120	0.087
2%Ga-Comm MFI	69	34	35	0.026	0.113	0.087
2%Zn-Comm MFI	100	46	54	0.028	0.119	0.091
Lamellar MFI	131	93	38	0.013	0.278	0.265
2%Ga-Lamellar MFI	128	101	27	0.010	0.249	0.239
2%Zn-Lamellar MFI	124	77	47	0.017	0.238	0.221

[a] Calculated from multi-point BET method.
[b] Calculated from *t*-plot method.
[c] Calculated from the adsorption isotherms at $p/p_0 = 0.99$.
[d] Calculated from $V_{meso} = V_{total} - V_{micro}$.

modification, the amount, nature, composition, and location of the coke deposits for ethylene conversion reaction can be controlled.

CRediT authorship contribution statement

Laleh Emdadi: Conceptualization, Methodology, Investigation, Writing - original draft, Visualization. **Luther Mahoney:** Investigation. **Ivan C. Lee:** Conceptualization. **Asher C. Leff:** Investigation. **Wei Wu:** . **Dongxia Liu:** Investigation. **Chi K. Nguyen:** Investigation. **Dat T. Tran:** Supervision.

Acknowledgements

Research was sponsored by the U.S. Army Research Laboratory and was accomplished under Cooperative Agreement Numbers W911NF-16-2-0008 and W911NF-16-2-0085. The views and conclusions contained in this document are those of the authors and should not be interpreted as representing the official policies, either expressed or implied, of the U.S. Army Research Laboratory or the U.S. Government. The U.S. Government is authorized to reproduce and distribute reprints for Government purposes notwithstanding any copyright notation herein. The authors would like to thank Dr. Pedro Castano for his advice and helpful suggestions regarding coke extraction technique and analysis of the FTIR data. Dr. Dongxia Liu and her student, Wei Wu, would like to thank for the support from National Science Foundation (CBET-1705284).

Appendix A. Supplementary data

Supplementary material related to this article can be found, in the online version, at doi:https://doi.org/10.1016/j.apcata.2020.117510.

References

[1] I. Amghizar, L.A. Vandewalle, K.M. Van Geem, G.B. Marin, Engineering 3 (2017) 171–178.
[2] A. Corma, J. Mengual, P.J. Miguel, Appl. Catal. A Gen. 417-418 (2012) 220–235.
[3] T. Ren, M.K. Patel, K. Blok, Energy 33 (2008) 817–833.
[4] F. Cherubini, Energy Conver. Manage. 51 (2010) 1412–1421.
[5] A. Galadima, O. Muraza, J. Ind. Eng. Chem. 31 (2015) 1–14.
[6] M. Guisnet, N.S. Gnep, D. Aittaleb, Y.J. Doyemet, Appl. Catal. A Gen. 87 (1992) 255–270.
[7] M. Inaba, K. Murata, M. Saito, I. Takahara, React. Kinet. Catal. Lett. 88 (2006) 135–141.
[8] D.B. Lukyanov, N.S. Gnep, M.R. Guisnet, Ind. Eng. Chem. Res. 33 (1994) 223–234.
[9] R. Barthos, A. Széchenyi, F. Solymosi, J. Phys. Chem. B 110 (2006) 21816–21825.
[10] X. Chen, M. Dong, X. Niu, K. Wang, G. Chen, W. Fan, J. Wang, Z. Qin, Chinese J. Catal. 36 (2015) 880–888.
[11] H. Coqueblin, A. Richard, D. Uzio, L. Pinard, Y. Pouilloux, F. Epron, Catal. Today 289 (2017) 62–69.
[12] A. Mehdad, R.F. Lobo, Catal. Sci. Technol. 7 (2017) 3562–3572.
[13] P. Qiu, J.H. Lunsford, M.P. Rosynek, Catal. Lett. 52 (1998) 37–42.
[14] V.R. Choudhary, P. Devadas, S. Banerjee, A.K. Kinage, Microporous Mesoporous Mater. 47 (2001) 253–267.
[15] F. Bauer, H.G. Karge, H.G. Karge, J. Weitkamp (Eds.), Characterization II, Springer, Berlin Heidelberg, Berlin, Heidelberg, 2007, pp. 249–364.
[16] M. Guisnet, F.R. Ribeiro, Deactivation and Regeneration of Zeolite Catalysts, Imperial College Press, 2011.
[17] H.G. Karge, H. van Bekkum, E.M. Flanigen, J.C. Jansen (Eds.), Studies in Surface Science and Catalysis, Elsevier, 1991, pp. 531–570.
[18] G.F. Froment, B. Delmon, G.F. Froment (Eds.), Studies in Surface Science and Catalysis, Elsevier, 1980, pp. 1–19.
[19] M. Guisnet, P. Magnoux, Appl. Catal. A: Gen.Appl. Catal. A Gen. 212 (2001) 83–96.
[20] M. Argyle, C. Bartholomew, Catalysts 5 (2015) 145–269.
[21] P. Castaño, G. Elordi, M. Olazar, A.T. Aguayo, B. Pawelec, J. Bilbao, Appl. Catal. B: Environ. 104 (2011) 91–100.
[22] M. Guisnet, P. Magnoux, Appl. Catal. 54 (1989) 1–27.
[23] M. Guisnet, P. Magnoux, E.G. Derouane, F. Lemos, C. Naccache, F.R. Ribeiro (Eds.), Springer, Dordrecht, Netherlands, 1992, pp. 457–474.
[24] M. Ibáñez, B. Valle, J. Bilbao, A.G. Gayubo, P. Castaño, Catal. Today 195 (2012) 106–113.
[25] B. Liu, D. Slocombe, M. AlKinany, H. AlMegren, J. Wang, J. Arden, A. Vai, S. Gonzalez-Cortes, T. Xiao, V. Kuznetsov, P.P. Edwards, Appl. Petrochem. Res. 6 (2016) 209–215.
[26] H.S. Cerqueira, C. Sievers, G. Joly, P. Magnoux, J.A. Lercher, Ind. Eng. Chem. Res. 44 (2005) 2069–2077.
[27] B. Liu, D.R. Slocombe, J. Wang, A. Aldawsari, S. Gonzalez-Cortes, J. Arden, V.L. Kuznetsov, H. AlMegren, M. AlKinany, T. Xiao, P.P. Edwards, Nat. Commun. 8 (2017) 514.
[28] J.E. Schmidt, J.D. Poplawsky, B. Mazumder, Ö. Attila, D. Fu, D.A.M. de Winter, F. Meirer, S.R. Bare, B.M. Weckhuysen, Angew. Chem. Int. Ed. 55 (2016) 11173–11177.
[29] A. Devaraj, M. Vijayakumar, J. Bao, M.F. Guo, M.A. Derewinski, Z. Xu, M.J. Gray, S. Prodinger, K.K. Ramasamy, Sci. Rep. 6 (2016) 37586.
[30] Á. Ibarra, A. Veloso, J. Bilbao, J.M. Arandes, P. Castaño, Appl. Catal. B: Environ. 182 (2016) 336–346.
[31] K.K. Ramasamy, Y. Wang, Catal. Today 237 (2014) 89–99.
[32] E. Epelde, M. Ibañez, A.T. Aguayo, A.G. Gayubo, J. Bilbao, P. Castaño, Microporous Mesoporous Mater. 195 (2014) 284–293.
[33] B. Valle, P. Castaño, M. Olazar, J. Bilbao, A.G. Gayubo, J. Catal. 285 (2012) 304–314.
[34] H. Zhang, S. Shao, R. Xiao, D. Shen, J. Zeng, Energy Fuels 28 (2014) 52–57.
[35] J. Goetze, B.M. Weckhuysen, Catal. Sci. Technol. 8 (2018) 1632–1644.
[36] Y. Jiang, J. Huang, J. Weitkamp, M. Hunger, R. Xu, Z. Gao, J. Chen, W. Yan (Eds.), Studies in Surface Science and Catalysis, Elsevier, 2007, p. 1137 1144.
[37] I. Kiricsi, I. Pálinkó, T. Kollár, J. Mol. Struct. 651-653 (2003) 331–334.
[38] C. Li, P.C. Stair, Catal. Today 33 (1997) 353–360.
[39] J. Li, G. Xiong, Z. Feng, Z. Liu, Q. Xin, C. Li, Microporous Mesoporous Mater. 39 (2000) 275–280.
[40] J.P. Lange, A. Gutsze, H.G. Karge, J. Catal. 114 (1988) 136–143.
[41] A.R. Pradhan, J.F. Wu, S.J. Jong, T.C. Tsai, S.B. Liu, Appl. Catal. A Gen. 165 (1997) 489–497.
[42] Y. Sang, A. Xing, C. Wang, Z. Han, Y. Wu, Catalysts 7 (2017) 171.
[43] F.L. Bleken, K. Barbera, F. Bonino, U. Olsbye, K.P. Lillerud, S. Bordiga, P. Beato, T.V.W. Janssens, S. Svelle, J. Catal. 307 (2013) 62–73.
[44] M. Choi, K. Na, J. Kim, Y. Sakamoto, O. Terasaki, R. Ryoo, Nature 461 (2009) 246.
[45] Y. Wu, L. Emdadi, S.C. Oh, M. Sakbodin, D. Liu, J. Catal. 323 (2015) 100–111.
[46] S.M. Holmes, A. Garforth, B. Maunders, J. Dwyer, Appl. Catal. A Gen. 151 (1997) 355–372.
[47] M. Ibáñez, M. Artetxe, G. Lopez, G. Elordi, J. Bilbao, M. Olazar, P. Castaño, Appl. Catal. B: Environ. 148-149 (2014) 436–445.
[48] L. Lakiss, F. Ngoye, C. Canaff, S. Laforge, Y. Pouilloux, Z. Qin, M. Tarighi, K. Thomas, V. Valtchev, A. Vicente, L. Pinard, J.-P. Gilson, C. Fernandez, J. Catal. 328 (2015) 165–172.
[49] F.F. Madeira, N.S. Gnep, P. Magnoux, H. Vezin, S. Maury, N. Cadran, Chem. Eng. J. 161 (2010) 403–408.
[50] K.K. Ramasamy, M.A. Gerber, M. Flake, H. Zhang, Y. Wang, Green Chem. 16 (2014) 748–760.
[51] S.-J. Jong, A.R. Pradhan, J.-F. Wu, T.-C. Tsai, S.-B. Liu, J. Catal. 174 (1998) 210–218.
[52] J. Oudar, Deactivation and Poisoning of Catalysts, Taylor & Francis, 1985.
[53] F. Schmidt, C. Hoffmann, F. Giordanino, S. Bordiga, P. Simon, W. Carrillo-Cabrera, S. Kaskel, J. Catal. 307 (2013) 238–245.
[54] D. Rojo-Gama, M. Signorile, F. Bonino, S. Bordiga, U. Olsbye, K.P. Lillerud, P. Beato, S. Svelle, J. Catal. 351 (2017) 33–48.
[55] S. Cheng, L. Wei, X. Zhao, J. Julson, Catalysts 6 (2016) 195.
[56] T.E. Tshabalala, N.J. Coville, M.S. Scurrell, Catal. Commun. 78 (2016) 37–43.
[57] N. Tsunoji, T. Sonoda, Y. Furumoto, M. Sadakane, T. Sano, Appl. Catal. A Gen. 481 (2014) 161–168.
[58] J. Kim, M. Choi, R. Ryoo, J. Catal. 269 (2010) 219–228.
[59] K. Lee, S. Lee, Y. Jun, M. Choi, J. Catal. 347 (2017) 222–230.
[60] R. Srivastava, M. Choi, R. Ryoo, Chem. Commun. (2006) 4489–4491.
[61] T. Cordero-Lanzac, A. Ateka, P. Pérez-Uriarte, P. Castaño, A.T. Aguayo, J. Bilbao, Ind. Eng. Chem. Res. 57 (2018) 13689–13702.
[62] M. Ibanez, P. Perez-Uriarte, M. Sanchez-Contador, T. Cordero-Lanzac, A.T. Aguayo, J. Bilbao, P. Castano, Catalysts 7 (2017) 254.
[63] J.C. Groen, T. Bach, U. Ziese, A.M. Paulaime-van Donk, K.P. de Jong, J.A. Moulijn, J. Pérez-Ramírez, J. Am. Chem. Soc. 127 (2005) 10792–10793.
[64] D.P. Serrano, J.M. Escola, P. Pizarro, Chem. Soc. Rev. 42 (2013) 4004–4035.
[65] Y. Wei, T.E. Parmentier, K.P. de Jong, J. Zecevic, Chem. Soc. Rev. 44 (2015) 7234–7261.
[66] K. Na, W. Park, Y. Seo, R. Ryoo, Chem. Mater. 23 (2011) 1273–1279.
[67] W.J. Roth, P. Nachtigall, R.E. Morris, J. Čejka, Chem. Rev. 114 (2014) 4807–4837.
[68] M. Tsapatsis, AIChE J. 60 (2014) 2374–2381.
[69] L. Mahoney, L. Emdadi, A.C. Leff, D.T. Tran, W. Wu, S. Cheng, D. Liu, C.K. Nguyen, I.C. Lee, Fuel 256 (2019) 115953.
[70] L. Emdadi, Y. Wu, G. Zhu, C.-C. Chang, W. Fan, T. Pham, R.F. Lobo, D. Liu, Chem. Mater. 26 (2014) 1345–1355.
[71] J.M. Ortega, A.G. Gayubo, A.T. Aguayo, P.L. Benito, J. Bilbao, Ind. Eng. Chem. Res. 36 (1997) 60–66.
[72] Y. Ji, H. Yang, W. Yan, Catalysts 7 (2017) 367.
[73] J. Kim, W. Kim, Y. Seo, J.-C. Kim, R. Ryoo, J. Catal. 301 (2013) 187–197.
[74] H.G. Karge, W. Nießen, H. Bludau, Appl. Catal. A Gen. 146 (1996) 339–349.
[75] J. Robertson, Mater. Sci. Eng. R Rep. 37 (2002) 129–281.
[76] M. Guisnet, L. Costa, F.R. Ribeiro, J. Mol, Catal. A: Chem. 305 (2009) 69–83.
[77] M. Hunger, Microporous Mesoporous Mater. 82 (2005) 241–255.
[78] J.W. Park, G. Seo, Appl. Catal. A Gen. 356 (2009) 180–188.
[79] O. Sánchez-Galofré, Y. Segura, J. Pérez-Ramírez, J. Catal. 249 (2007) 123–133.